

## Acquisition of Powder Diffraction Data with Synchrotron Radiation\*

D. E. Cox,<sup>A</sup> B. H. Toby<sup>B</sup> and M. M. Eddy<sup>C</sup>

<sup>A</sup> Department of Physics, Brookhaven National Laboratory,  
Upton, NY 11973, U.S.A.

<sup>B</sup> Central Scientific Laboratory, Union Carbide Corporation,  
Tarrytown, NY 10951, U.S.A.

<sup>C</sup> Department of Chemistry, University of California  
at Santa Barbara, Santa Barbara, CA 93106, U.S.A.

### *Abstract*

During the past year, a dedicated triple-axis powder diffractometer has been in routine operation at the Brookhaven National Synchrotron Light Source as a user-oriented facility. The diffractometer is designed to allow easy interchange between energy-dispersive and monochromatic beam experiments. In the latter mode of operation, high resolution data have been collected for a variety of samples with the use of the crystal-analyser technique, and in several cases these data sets have been used successfully for structure solution and Rietveld refinement. Several aspects of data acquisition at a synchrotron beam-line are described, and some of the different types of scattering geometry which have been used are discussed. Simple expressions are given for the instrumental resolution function expressed as the angular variation of peak widths for each of these. The peak shapes observed for a reference sample of Si on the present triple-axis instrument are well described by the convolution of Gaussian and Lorentzian functions, and the angular dependence of the Gaussian component is in excellent agreement with the corresponding calculated instrumental function. One of the most important considerations for each type of experiment is the necessary compromise between intensity and resolution over a wide range of scattering angles, and some of the available options are discussed. In particular, the use of Ge(440) and LiF(400) analyser crystals gives a focussing minimum at relatively high angles ( $2\theta \approx 50^\circ$  at  $1.54 \text{ \AA}$ ), a highly desirable feature for Rietveld analysis of complex structures. Absolute intensities from reference samples of Si and  $\text{CeO}_2$  are calculated for these and several other scattering configurations involving both flat-plate and capillary geometry to illustrate this compromise.

### 1. Introduction

Synchrotron X-ray powder diffraction is rapidly evolving as a powerful technique for structural studies, and several papers dealing with structure determination have recently appeared or are in press. In many ways the situation resembles that of neutron powder diffraction a decade ago, and a dramatic increase in the use of synchrotron techniques is to be expected as more high-brightness sources and dedicated powder instruments become available.

The high resolution and peak-to-background intensity ratios (better than 1000:1 in many cases) and the high accuracy with which the low-angle peak positions can be determined (typically to better than  $0.005^\circ$ ) are particularly well suited to

\* Paper presented at the International Symposium on X-ray Powder Diffractometry, held at Fremantle, Australia, 20-23 August 1987.

the application of automatic indexing methods when the unit cell is unknown, to subsequent structure solution by *ab initio* techniques, and finally to the refinement of complex structures by the Rietveld (1969) profile technique. In addition, the high photon flux and continuous spectral distribution are useful for anomalous scattering experiments, and can also be very effectively exploited for energy-dispersive diffraction studies of exceedingly small samples ( $\approx 10^{-9}$  cm<sup>3</sup>) in diamond-anvil cells at ultra-high pressures ( $>1$  Mbar or  $>10^5$  MPa).

In the present paper, some of the aspects of data acquisition with synchrotron radiation are described in detail based upon the experience gained during about one year's continuous operation of the dedicated triple-axis powder diffractometer situated at beam-line X13A at the Brookhaven National Synchrotron Light Source (NSLS). This instrument is designed to allow easy interchange between monochromatic and energy-dispersive modes of operation, and has been described in detail in a recent publication (Cox *et al.* 1986).

The present paper is restricted to powder diffraction with a monochromatic beam. As always in diffraction experiments of this type, it is necessary to compromise between intensity and resolution over a wide range of scattering angles, and this is discussed in detail for the different experimental arrangements reported in the literature to date.

For the analysis of complex structures, one important point well known to neutron diffractionists is the desirability of tailoring the resolution function to the density of peaks in the pattern by exploiting the focussing properties of a crystal monochromator, as first emphasised by Hewat (1975). This requires the diffractometer to be designed so that the best angular resolution occurs at higher values of  $2\theta$  where the density of peaks is greatest, and similar considerations apply to X-ray diffractometers. However, for other applications, such as materials characterisation, phase equilibrium studies, automatic indexing of unknown unit cells and line profile analysis, the best angular resolution is more likely to be needed at lower angles. One of the advantages of the synchrotron is that the very high intensity allows great flexibility in the choice of experimental conditions.

## 2. General Aspects of Data Acquisition

One of the advantages of powder diffraction experiments is the underlying simplicity of the technique. There is no intrinsic reason why data acquisition at a dedicated synchrotron X-ray diffractometer should be any more difficult than with laboratory equipment and this has in fact been found to be the case at X13A. The very simple optics of the beam-line have proved to be remarkably insensitive to various fluctuations in the beam orbit which have affected some of the more sophisticated instruments. In particular, for many months it has been routine to leave long scans in progress overnight completely unattended and under computer control. Full data sets have been collected over as many as four separate beam fills without any indication of discontinuities.

Most of the hardware required for powder diffraction experiments is similar to that used in the laboratory and will not be discussed in detail, nor will monochromators and mirrors, which have been covered in many other publications. A vertically scattering double crystal Ge(111) monochromator with horizontal sagittal focussing is probably a good choice for most purposes, and should give of the order of  $10^{11}$  photons/s at the sample position. The present configuration at X13A consists of

a horizontally scattering single flat Ge(111) monochromator, and the scattering from the sample is measured in the vertical plane. To insure high resolution, no more than 0.25 mrad of the horizontal radiation fan is used in typical experiments, giving about  $2 \times 10^{10}$  photons/s at the sample position for wavelengths of 1.3–1.5 Å for a stored beam of 100 mA at 2.5 GeV, and an energy resolution  $\Delta E/E \approx 10^{-3}$ .

The incident beam is defined by a slit system consisting of four tantalum masks independently moved by stepping motors under computer control with a resolution of 2.5  $\mu\text{m}$ . This has proved to be a very valuable feature, particularly when small incident beams are required. An ion chamber filled with flowing  $\text{N}_2$  is used in conjunction with a current-to-voltage amplifier and a voltage-to-frequency converter to monitor the incident beam. This has the advantage over a scattered beam monitor of allowing a fairly accurate determination of the incident photon intensity and provides a means for making absolute measurements if desired.

For most of the monochromatic beam experiments high resolution is obtained with a perfect crystal analyser in the diffracted beam. As described in detail earlier (Cox *et al.* 1983; Hastings *et al.* 1984) this can be regarded as a very narrow 'angular' receiving slit with an effective divergence of less than  $0.01^\circ$  and a band-pass of a few eV, which serves to reject any unwanted fluorescence radiation and allows very high peak-to-background counting ratios to be obtained with well-crystallised samples. The low background is a very important feature, since it is thereby possible to detect extremely weak peaks and also extract maximum information about peak shapes. Another advantage of the crystal-analyser technique is the accuracy with which the peak positions can be determined (frequently to within  $0.002^\circ$ ) due to the absence of displacement-type effects. This latter feature allows wide-diameter (up to 2 mm) capillary samples to be used with no loss of resolution provided, of course, that absorption losses are not too large.

A standard scintillation detector with an aperture of  $13 \times 4.5$  mm is placed close to the analyser and the whole assembly carefully shielded with lead. With the detector situated 70 cm from the sample, asymmetric broadening of the low-angle peaks due to axial divergence effects is reduced to an acceptably low level without the use of a Soller collimator.

Data are collected in the usual fashion by step-scanning under computer control at appropriate step intervals (usually in the range  $0.005$ – $0.02^\circ$ ). Because of the extremely small divergence of the incident beam it is absolutely essential to rotate or oscillate the sample to achieve proper averaging over a sufficiently large number of particles. At X13A this is achieved by oscillation of the sample (both flat-plate and capillary) about the horizontal axis perpendicular to the scattering plane over a range of a few degrees. This has been found to give reproducible integrated intensities to within 1–2%, and should be especially convenient for samples mounted in furnaces or cryostats, since there is usually no difficulty in oscillating the whole chamber assembly over small ranges.

More conventional types of scattering geometry which do not involve an analyser are possible, of course, and two have been described in detail in the literature. Parrish *et al.* (1986*b*) have carried out a series of experiments on reference samples at the Stanford Synchrotron Radiation Laboratory (SSRL) with a channel-cut Si(111) monochromator, flat-plate samples in both reflection and transmission geometry, and narrow incident beam and receiving slits with an overall divergence of around  $0.1$ – $0.2^\circ$ . This type of geometry allows much higher intensities to be obtained, but

gives considerably broadened peaks. In subsequent experiments (Parrish and Hart 1985; Parrish *et al.* 1986*a*), the receiving slit was replaced by a Soller collimator with a divergence of  $0.17^\circ$ .

Christensen *et al.* (1985) and Lehmann *et al.* (1987) have carried out experiments at the Hamburg Synchrotron-Strahlungslabor (HASYLAB) in which a double crystal Ge(111) monochromator was used in conjunction with a narrow diameter capillary sample and a commercial linear position-sensitive detector. This arrangement allows fairly rapid collection of high resolution data (1–2 hours for a complete scan) and has been successfully exploited for complex structure refinement. However, the peak-to-background discrimination may not be so good, particularly if the sample fluoresces.

In the following sections, some simple expressions for the resolution of a variety of different arrangements are given, together with some estimates of integrated intensities and peak counting rates. These results are then compared with some recent experimental results obtained at X13A.

### 3. Resolution Expressions

The first case to be considered is that of a double-crystal monochromator and sample scattering in the vertical plane in non-dispersive geometry, with a Soller collimator in the scattered beam. It is straightforward to derive the following approximate expression for the variation of  $\Gamma$ , the peak full-width at half-maximum as a function of  $2\theta$ :

$$\Gamma = \{\phi_V^2(2 \tan \theta / \tan \theta_M - 1)^2 + \delta^2\}^{\frac{1}{2}}, \quad (1)$$

where  $\phi_V$  is the vertical divergence of the incident beam (typically  $0.01$ – $0.02^\circ$ ),  $\theta_M$  is the monochromator angle and  $\delta$  is the divergence of the collimator, defined as the spacing between the foils divided by the length of the collimator (i.e. total reflection effects are neglected). The above formula neglects the small contribution from the Darwin width of the monochromator and any broadening due to axial divergence or displacement-type effects. It may be noted that equation (1) is readily derived from the expressions worked out for the double-axis neutron powder diffractometer by Caglioti *et al.* (1958), with  $\alpha_1 = \phi_V$ ,  $\alpha_2 = 0$ ,  $\alpha_3 = \delta$  and  $\beta = 0$ , and gives a focussing minimum at  $2 \tan \theta = \tan \theta_M$ . For Si(111) and Ge(111) monochromators at typical wavelengths of  $1.0$ – $1.5 \text{ \AA}$ , this minimum occurs at relatively low values of  $2\theta$  in the range  $10$ – $15^\circ$ . As mentioned earlier, for structure analysis and refinement, it is often more desirable for this minimum to be at a much higher angle, and one possible solution would be to use Si or Ge in the (333) setting. A second point to be noted is that  $\Gamma$  at the focussing position ( $\Gamma_{\min}$ ) is controlled by the Soller collimator divergence  $\delta$ . For high resolution this should be made comparable to  $\phi_V$ , i.e.  $0.01$ – $0.02^\circ$ , a far from easy task, particularly when total reflection effects are considered.

Equation (1) is also valid when a position-sensitive detector (PSD) or a conventional receiving slit is used in the diffracted beam. In this case we have

$$\delta \approx (w_S^2 + w_R^2)^{\frac{1}{2}} / D_{SR},$$

where  $w_S$  and  $w_R$  are respectively the width or diameter of the sample (or the incident

beam in the case of extended flat-plate geometry) and the width of the receiving slit (or the spatial resolution of the PSD), and  $D_{SR}$  is the distance between the sample and the receiving slit (or PSD). Thus if  $w_S$  and  $w_R$  are 0.2 mm and  $D_{SR}$  is 1 m,  $\delta$  is about 0.02°.

In all of these cases, the peak profile should be approximately Gaussian in shape if there are no sample broadening effects. From the Scherrer formula  $\Delta 2\theta \approx \lambda/L \cos \theta$ , this implies a mean particle size  $L$  of at least 2  $\mu\text{m}$ .

When a perfect analyser crystal is used in the diffracted beam, the following expression may be derived for non-dispersive geometry:

$$\Gamma = \{ \phi_V^2 (2 \tan \theta / \tan \theta_M - \tan \theta_A / \tan \theta_M - 1)^2 + \Gamma_{\min}^2 \}^{\frac{1}{2}}. \quad (2)$$

This is a slightly modified version of the expression given by Hastings *et al.* (1984) which includes a constant term  $\Gamma_{\min}$  to allow for small contributions from the Darwin widths of the monochromator and analyser. Once again, this formula may be derived from the equations for a triple-axis neutron diffractometer obtained by Caglioti and Tocchetti (1965) with appropriate simplifications.

An important difference between equations (2) and (1) is that the focussing minimum now occurs when  $2 \tan \theta = \tan \theta_A + \tan \theta_M$ . This provides a very convenient way to vary the instrumental resolution over a wide range of conditions, since in general it is much easier to change the analyser crystal or its setting than the monochromator.

For the arrangement used at X13A, namely a single crystal scattering in the horizontal plane, a slightly modified form of equation (2) applies:

$$\Gamma = \{ \phi_H^2 (2 \tan \theta / \tan \theta_M - \tan \theta_A / \tan \theta_M)^2 + \Gamma_{\min}^2 \}^{\frac{1}{2}}, \quad (3)$$

and the corresponding focussing condition is  $2 \tan \theta = \tan \theta_A$ . Here  $\phi_H$  is the horizontal divergence defined by incident beam slits and the horizontal source size.

**Table 1.** Selected properties of three different analysers used at X13A ( $\lambda = 1.32 \text{ \AA}$ )  
Here  $R_{\text{calc}}$  is the integrated reflectivity calculated from equation (12) and normalised to the value for Ge(440), and  $R_{\text{obs}}$  is the average value found for several reflections from the Si reference sample

	$d \text{ (\AA)}$	$\theta_A \text{ (deg.)}$	$R_{\text{calc}}$	$R_{\text{obs}}$
Ge(220)	2.0002	19.27	2.4	2.8
Ge(440)	1.0001	41.29	1.0	1.0
LiF(400)	1.0066	40.97	0.3	4.6

#### 4. Experimental Tests of Resolution at X13A

Since the exploratory experiments at the Cornell High Energy Synchrotron Source (CHESS) reported by Cox *et al.* (1983) and Hastings *et al.* (1984) with a vertically scattering double-crystal Si monochromator and a Ge(111) analyser, several different monochromator-analyser configurations have been tried at X13A, and the variation of peak widths and shapes has been studied in considerable detail.

For the experiments described here, a Ge(111) monochromator situated 15.7 m from the source scattering horizontally at a wavelength of about 1.32  $\text{\AA}$  ( $\theta_M = 11.66^\circ$ )

was used, with the three different analysers Ge(220), Ge(440) and LiF(400). The latter is in fact not perfect, but is known to have a narrow mosaic spread of about  $0.01^\circ$ . Some relevant details for these crystals are summarised in Table 1. The beam size was approximately 4 mm wide by 1.5 mm high, corresponding to a horizontal divergence of about  $0.015^\circ$ , and the intensity at the sample position was about  $2 \times 10^{10}$  photons/s for a stored current of 100 mA, with  $\Delta E/E$  about  $1.2 \times 10^{-3}$ . The reference sample was a pressed disc of Si powder in flat-plate geometry. SEM pictures reveal this sample to have a crystallite size of around 5–20  $\mu\text{m}$ , and the Scherrer broadening is therefore expected to be negligible ( $\approx 0.001^\circ$ ). Data were obtained by step-scanning selected peaks while the sample was oscillated over a range of  $4^\circ$  for the lower angle peaks and  $8^\circ$  for the others. The maximum counting rates recorded were around  $10^4$  counts/s.

Individual least-squares fits to the data were made with a pseudo-Voigt peak shape function (Young and Wiles 1982) which has the form

$$I(\Delta 2\theta) = I_0 [C_L \eta \{1 + 4(\Delta 2\theta/\Gamma)^2\}^{-1} + C_G(1-\eta) \exp\{-4 \ln 2(\Delta 2\theta/\Gamma)^2\}], \quad (4)$$

where  $I_0$  is the integrated intensity,  $\Delta 2\theta$  is the displacement from the peak maximum  $2\theta_0$ ,  $\eta$  is a mixing parameter and  $C_L$  and  $C_G$  are the normalisation constants  $2/\pi\Gamma$  and  $2(\ln 2/\pi)^{1/2}/\Gamma$  respectively. This function provides a good approximation to the convolution of Lorentzian and Gaussian functions with half-widths  $\Gamma_L$  and  $\Gamma_G$  respectively (Wertheim *et al.* 1974). Six parameters were refined for each peak:  $I_0$ ,  $\Gamma$ ,  $2\theta_0$ ,  $\eta$  and background values on either side of the peak,  $B_L$  and  $B_H$ , with linear interpolation in between. As previously noted (Cox *et al.* 1986), this function accounts very well for the peak shapes of well-crystallised reference samples such as Si and  $\text{CeO}_2$ . The half-widths  $\Gamma_L$  and  $\Gamma_G$  may be obtained from the refined values of  $\Gamma$  and  $\eta$  via the following polynomial approximations derived from a set of computer-generated convolutions:

$$\Gamma_L = 0.72928\eta + 0.19289\eta^2 + 0.07783\eta^3, \quad (5)$$

$$\Gamma_G = (1 - 0.74417\eta - 0.24781\eta^2 - 0.00810\eta^3)^{1/2}. \quad (6)$$

The results for the three analysers are shown in Fig. 1. Least-squares fits of  $\Gamma_G$  to equation (3) with  $\phi_H$  and  $\Gamma_{\min}$  as variables are shown by the dotted lines, and the refined values of the variables are listed in Table 2. In each case,  $\phi_H$  is in good agreement with the experimental value, while  $\Gamma_{\min}$  is about  $0.01^\circ$ . The effects of focussing are very well demonstrated for the Ge(440) and LiF(400) analysers, with a pronounced minimum at the expected value of  $2\theta$ .

Fig. 1 also shows that there is a significant Lorentzian component present in each case which is a smoothly increasing function of  $2\theta$ . The broken lines in Fig. 1 show least-squares fits to the expression

$$\Gamma_L = X \tan \theta + Y/\cos \theta, \quad (7)$$

which has been found to be a good approximation in a number of Rietveld analyses. Here  $X$  and  $Y$  are refinable parameters, and  $Y$  can be readily related to the particle

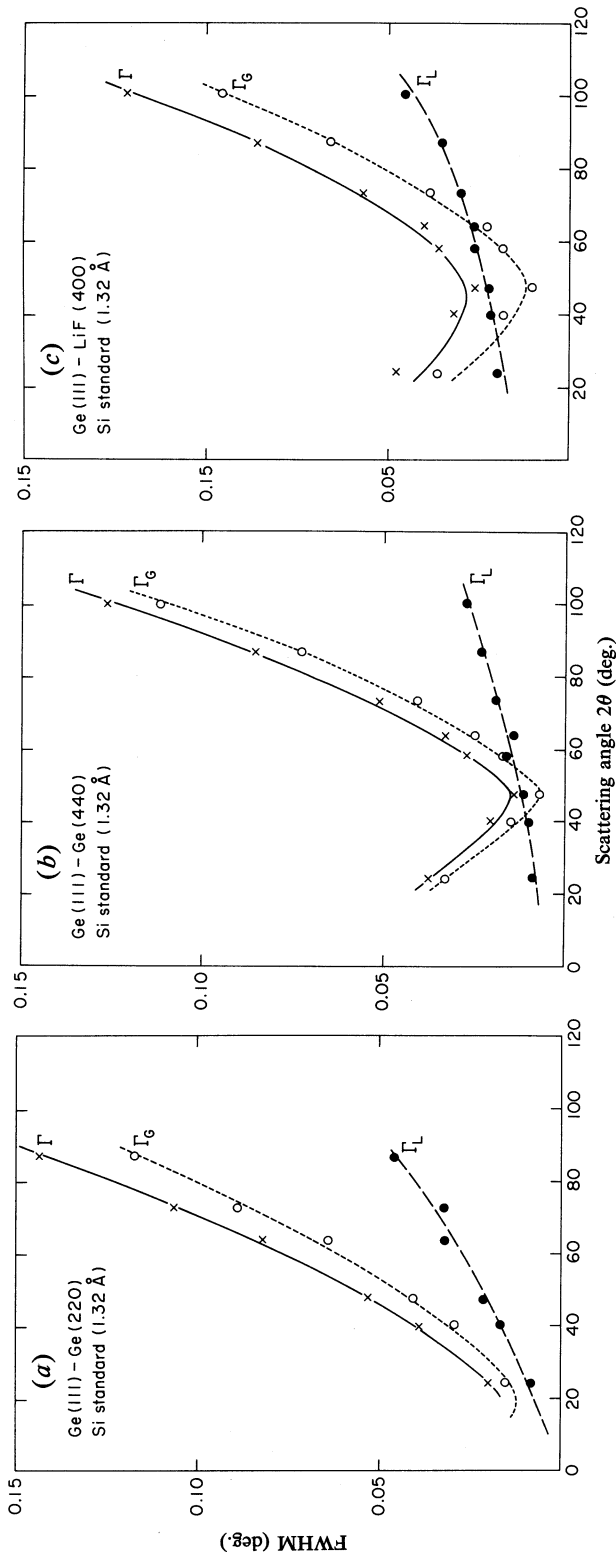


Fig. 1. Variation of Lorentzian  $\Gamma_L$ , Gaussian  $\Gamma_G$  and overall  $\Gamma$  peak widths for a Ge(111) monochromator scattering horizontally at 1.54 Å and three different analysers (a) Ge(220), (b) Ge(440) and (c) LiF(400) as discussed in Section 4. The closed circles, open circles and crosses are experimental values of  $\Gamma_L$ ,  $\Gamma_G$  and  $\Gamma$  obtained by individual least-squares fits to the pseudo-Voigt function in equation (4). The broken and dotted lines show least-squares fits of  $\Gamma_L$  and  $\Gamma_G$  to equations (7) and (3) respectively, and the solid line shows  $\Gamma$  calculated from equation (8).

size. Since no particle size broadening is expected for this sample,  $Y$  should be close to zero, and the refined values listed in Table 2 show this is indeed the case for Ge(220) and Ge(440), but not for LiF(400), for which  $Y$  is about  $0.01^\circ$ . This is probably related to the fact that this crystal has a small mosaic spread of about this amount, also evident from the observed reflectivity, which is about an order of magnitude greater than that calculated for a perfect crystal (Table 1). Since the overall resolution is only slightly inferior to that of Ge(440), and the reflectivity is almost five times higher, this crystal has been used extensively for the collection of data sets for Rietveld analysis.

**Table 2.** Results of least-squares fits of  $\phi_H$  and  $\Gamma_{\min}$  to equation (3) and  $X$  and  $Y$  to equation (7) for a Ge(111) monochromator ( $\lambda = 1.32 \text{ \AA}$ ) and the three analysers discussed in Section 4

Numbers in parentheses are e.s.d. values referred to the least significant digit. The experimental value of  $\phi_H$  is estimated to be  $0.016^\circ$

	Ge(220)	Ge(440)	LiF(400)
$\phi_H$ (deg.)	0.0154(3)	0.0148(2)	0.0128(4)
$\Gamma_{\min}$ (deg.)	0.012(3)	0.006(2)	0.012(2)
$X$ (deg.)	0.050(5)	0.018(2)	0.018(2)
$Y$ (deg.)	-0.002(2)	0.004(1)	0.014(1)

Table 2 shows that  $\Gamma_L$  has a predominantly  $\tan\theta$  dependence with  $X$  about  $0.02^\circ$  for Ge(440) and LiF(400), but significantly more for Ge(220). The physical significance of this term is not clear at this stage, but it was not observed to this extent in previous experiments at CHESS with a double crystal monochromator (Cox *et al.* 1983; Hastings *et al.* 1984; Thompson *et al.* 1987) and may result from the scattering geometry. Detailed calculations of the resolution function are needed to check this point.

These results show clearly that equations (3) and (7) not only provide a very satisfactory description of the observed instrumental resolution function but also allow sample broadening effects due to particle size or strain to be included in a physically plausible way. This is an important point for Rietveld analysis, and a practical illustration is provided by the results in recent Rietveld refinements of the structure of  $\alpha$ -CrPO<sub>4</sub> (Attfield *et al.* 1986*a*, 1986*b*) and quartz (McKeown *et al.* 1986). The program used was a locally modified version of the Rietveld code (Rietveld 1969; Hewat 1973) in which  $\Gamma_G = (U \tan^2 \theta + V \tan \theta + W)^{1/2}$  and  $\Gamma_L$  is given by equation (7). Both sets of data were taken on samples loaded into 1 mm capillaries under approximately the same conditions as above, with Ge(220) and Ge(440) analysers for  $\alpha$ -CrPO<sub>4</sub> and quartz respectively. Fig. 2 shows the curves for  $\Gamma_G$  and  $\Gamma_L$  calculated from the refined values of  $U$ ,  $V$ ,  $W$ ,  $X$  and  $Y$ , and also the curve for  $\Gamma$  calculated from the polynomial approximation

$$\Gamma = (\Gamma_G^5 + 2.69269 \Gamma_G^4 \Gamma_L + 2.42843 \Gamma_G^3 \Gamma_L^2 + 4.47163 \Gamma_G^2 \Gamma_L^3 + 0.07842 \Gamma_G \Gamma_L^4 + \Gamma^5)^{0.2}, \quad (8)$$

derived from a set of computer generated convolutions.

It can be seen from Fig. 2 that the curves obtained for  $\Gamma_G$  are very similar to those in Figs 1a and 1b, and clearly reflect the instrumental resolution. The most striking difference is seen in the  $\Gamma_L$  curve for quartz, which is dominated by a Scherrer-like term with an intercept at  $2\theta = 0^\circ$  of about  $0.04^\circ$ , corresponding to a mean particle size of about  $0.2 \mu\text{m}$ .

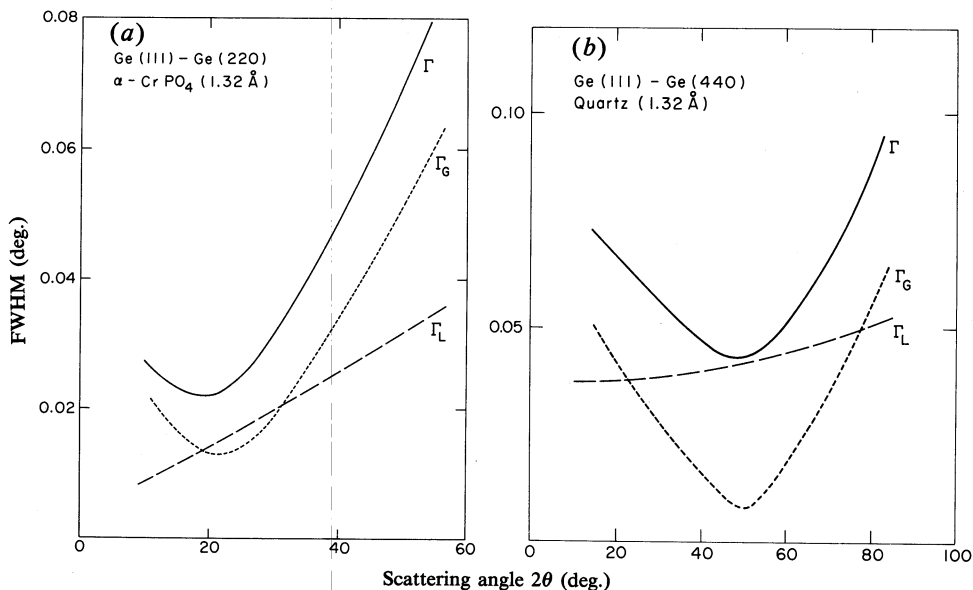
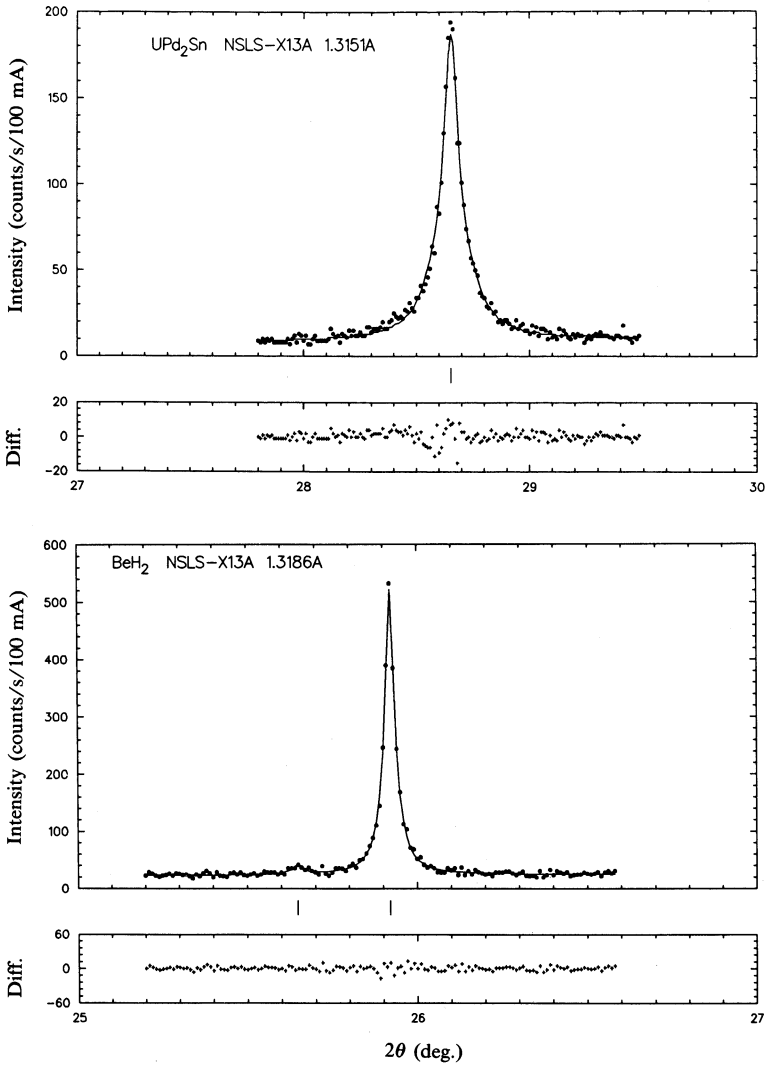


Fig. 2. Variation of  $\Gamma_L$ ,  $\Gamma_G$  and  $\Gamma$  obtained in Rietveld structure refinements of (a)  $\alpha\text{-CrPO}_4$  and (b) quartz. Note by comparison with Figs 1a and 1b that  $\Gamma_G$  is essentially resolution-limited with a well-defined minimum in each case, corresponding to the focussing conditions of equation (3).

The available data for other scattering configurations in which no analyser is used are relatively sparse. From Rietveld refinement of the structure of  $\text{Al}_2\text{Y}_4\text{O}_9$  with data collected from a capillary sample and a PSD, Lehmann *et al.* (1987) have derived curves for  $\Gamma$  against  $2\theta$  which conform closely to those calculated from equation (1) with the experimental values of  $\phi_V = 0.27 \text{ mrad}$  and  $\delta = 0.4 \text{ mrad}$ .

Most of the data reported by Parrish and co-workers have been obtained with relatively wide divergence slits ( $\approx 0.1\text{--}0.2^\circ$ ). Under these conditions the peak widths are dominated by the  $\delta^2$  term in equation (1) and do not show any evidence of a focussing minimum.

One final word of caution concerning peak shapes is illustrated by the data shown in Fig. 3, which shows profile fits and difference plots for the (112) reflection from  $\text{UPd}_2\text{Sn}$  (Marezio *et al.* 1988) and the (202) reflection from  $\text{BeH}_2$  (Smith *et al.* 1987). Least-squares fits to these peaks based upon the pseudo-Voigt function of equation (4) with two background variables converged satisfactorily to a very respectable goodness-of-fit index in each case, but with values of  $\eta$  significantly greater than unity, 1.27(5) and 1.15(6) respectively. The data extended over ranges of  $18\Gamma$  and  $40\Gamma$  respectively, and correlations between  $\eta$  and the two background variables were very small. This kind of 'super-Lorentzian' peak shape was also found for most of the other peaks. A detailed account of the Rietveld refinement of these structures will



**Fig. 3.** Peak fits and difference plots for (*top*) the (112) reflection from UPd<sub>2</sub>Sn and (*bottom*) the (202) reflection from BeH<sub>2</sub>, obtained with the pseudo-Voigt function of equation (4). The refined values of  $\Gamma$  and  $\eta$  were 0.095(5) and 1.27(5) (*top*) and 0.035(2) and 1.15(6) (*bottom*), with weighted goodness-of-fit (chi-squared) indices of 1.25 and 1.12 respectively. Short vertical markers represent the peak positions. The weak peak at  $2\theta = 25.64^\circ$  (*bottom*) is due to an unidentified impurity.

be given in forthcoming papers, but it is clear that there is much to be learned about profile broadening effects from high resolution synchrotron data.

## 5. Absolute Intensity Expressions

The detailed derivations of formulae for the integrated intensity of powder diffraction peaks may be found in a number of standard texts. The expression given by Suortti *et al.* (1985) is particularly convenient for the present discussion of absolute intensities.

For an extended flat-plate sample in reflection geometry, the integrated intensity  $I$  obtained in a step-scan may be expressed as

$$I = I_0 \left( \frac{e^2}{mc^2} \right)^2 \frac{N^2 \lambda^3 j |F e^{-M}|^2}{8\pi \sin \theta \sin 2\theta} A K_{\text{pol}} \Delta\phi \Delta\psi, \quad (9)$$

where  $I = \sum_n i(2\theta) \Delta(2\theta)$ , i.e. the net cumulative count in the detector multiplied by the step size (corrected for background),  $I_0$  is the number of photons incident on the sample for each step,  $e^2/mc^2$  is the classical electron radius ( $0.2818 \times 10^{-12}$  cm),  $N$  is the number of unit cells per unit volume,  $A$  is the absorption factor,  $K_{\text{pol}}$  the polarization factor,  $\Delta\phi$  the axial and  $\Delta\psi$  the equatorial opening of the receiving slit. The other quantities have their usual significance. For samples which satisfy the usual 'infinitely thick' criterion, we have  $A = 1/2\mu$ . If a Soller collimator with divergence  $\delta$  is used to reduce the axial divergence of the diffracted beam,  $\Delta\phi \approx \delta$ ; otherwise  $\Delta\phi \approx l_{\text{R}}/D_{\text{SR}}$ , where  $l_{\text{R}}$  is the length of the receiving slit (or detector aperture) and  $D_{\text{SR}}$  its distance from the sample. As discussed below,  $K_{\text{pol}}$  and  $\Delta\psi$  will depend upon the type of scattering geometry used.

The corresponding expression for a cylindrical sample in Debye-Scherrer geometry is

$$I = I_0 \left( \frac{e^2}{mc^2} \right)^2 \frac{N^2 \lambda^3 j |F e^{-M}|^2}{8\pi \sin \theta \sin 2\theta} V A K_{\text{pol}} \Delta\phi \Delta\psi, \quad (10)$$

where  $I_0$  is now the number of photons *per unit area* incident on the sample for each step and  $V$  is the sample volume. The absorption factor  $A$  is now a function of  $2\theta$  and may be obtained by numerical integration (Kasper and Lonsdale 1959). For relatively small values of  $\mu R$  ( $R$  is the sample radius), it is worth noting that  $A$  has a form very much like that of a temperature factor (Rouse *et al.* 1970; Hewat 1979).

The values of  $K_{\text{pol}}$  and  $\Delta\psi$  depend upon whether an analyser crystal is used or not. For a single receiving slit of width  $w_{\text{R}}$  and distance  $D_{\text{SR}}$  from the sample with no analyser in place,  $\Delta\psi = w_{\text{R}}/D_{\text{SR}}$  and

$$K_{\text{pol}} = (I_{0,\perp} + I_{0,\parallel} \cos^2 2\theta)/I_0, \quad (11)$$

where  $I_{0,\perp}$  and  $I_{0,\parallel}$  are the components of  $I_0$  perpendicular and parallel to the scattering plane respectively. These components can be measured either directly by a simple powder diffraction technique or calculated from the machine optics (Materlik and Suortti 1984). For vertical scattering geometry,  $I_{0,\parallel}$  is generally a few per cent of  $I_0$ . If a Soller collimator with equatorial divergence  $\delta$  is used instead of a narrow receiving slit, then  $\Delta\psi = \delta$ . These expressions are also valid for a PSD with spatial resolution  $w_{\text{R}}$  if the step-size  $\Delta 2\theta$  is replaced by  $\Delta\psi$ . The sum  $\sum i$  is now a direct measure of the integrated intensity.

If an analyser crystal is used, the equatorial opening is determined by the integrated reflectivity (Suortti *et al.* 1985), which for a perfect crystal in the limit of zero absorption is given by

$$\Delta\psi = \int R^\theta d\theta = \frac{8}{3\pi} \frac{e^2}{mc^2} \frac{N\lambda^2 |F' e^{-M}|}{\sin 2\theta} (I_{0,\perp} + I_{0,\parallel} |\cos 2\theta_{\text{A}}|)/I_0, \quad (12)$$

where  $\theta_A$  is the analyser angle. The polarisation term is given by

$$K_{\text{pol}} = (I_{0,\perp} + I_{0,\parallel} |\cos 2\theta_A| \cos^2 2\theta) / I_0. \quad (13)$$

If a narrow-mosaic crystal analyser is used,  $\cos 2\theta_A$  should be replaced in the expression for  $K_{\text{pol}}$  by a term  $K = \cos^n 2\theta_A$ , where  $K$  can be either greater or less than  $\cos 2\theta_A$  (Jennings 1984) depending on the experimental conditions. Since  $n$  is generally found to be fairly close to unity,  $K$  is taken as  $\cos 2\theta_A$  for the present purposes. The integrated reflectivity  $\Delta\psi$  may be determined by direct measurement if required.

The remaining quantity of interest is the peak intensity  $I_p$ . If  $\Delta\psi$  is reasonably small compared with  $\Gamma$ ,  $I_p$  is given by

$$I_p = CI/\Gamma = C \sum i(2\theta) \Delta 2\theta / \Gamma, \quad (14)$$

where  $C$  is a normalisation constant which depends upon the degree of Gaussian and Lorentzian character and lies between  $2(\ln 2/\pi)^{1/2}$  and  $2/\pi$  at the two extremes; for a rough estimate  $C$  can be taken as 0.8.

**Table 3.** Calculated absolute intensities  $\Sigma i$  and peak counting rates  $I_p$  for reference samples of (a) Si and (b) CeO<sub>2</sub> from equations (9)–(14) (see Section 6)

Here  $I_0 = 2 \times 10^{10}$  photons/s, beam width is 4 mm, beam height is 1 mm,  $\lambda = 1.54 \text{ \AA}$ ,  $I_{0,\perp}/I_0 = 0.97$  and  $I_{0,\parallel}/I_0 = 0.03$ . For step-scans,  $\Delta 2\theta$  is taken as  $0.01^\circ$ . Temperature factors for Si, CeO<sub>2</sub> and Ge are assumed to be  $0.5 \text{ \AA}^2$ . RS denotes a receiving slit 0.2 mm wide and PSD denotes a position-sensitive detector with 0.1 mm resolution, both at a distance of 70 cm from the sample. Detector aperture is taken as 1.3 cm ( $\Delta\phi = 0.0186$ )

	RS FP	PSD 0.2 mm cap	Ge(220)		LiF(400)	
			FP	1.0 mm cap	FP	1.0 mm cap
(a) Si						
$\Gamma$ (deg.)	0.089	0.035	0.042	0.042	0.041	0.041
$\Delta\psi$ (deg.)	0.0164	0.0082	0.0044	0.0044	0.0072 <sup>A</sup>	0.0072 <sup>A</sup>
$\Sigma i$ (photons/s)	$1.9 \times 10^5$	$1.5 \times 10^4$	$5.0 \times 10^4$	$2.0 \times 10^4$	$8.1 \times 10^4$	$3.2 \times 10^4$
$I_p$ (photons/s)	$1.7 \times 10^4$	$2.9 \times 10^3$	$9.5 \times 10^3$	$3.8 \times 10^3$	$1.6 \times 10^4$	$6.3 \times 10^3$
(b) CeO <sub>2</sub>						
$\Gamma$ (deg.)	0.089	0.035	0.042	0.042	0.041	0.041
$\Delta\psi$ (deg.)	0.0164	0.0082	0.0044	0.0044	0.0072 <sup>A</sup>	0.0072 <sup>A</sup>
$\Sigma i$ (photons/s)	$1.0 \times 10^5$	$2.2 \times 10^3$	$2.7 \times 10^4$	$1.0 \times 10^3$	$4.4 \times 10^4$	$1.6 \times 10^3$
$I_p$ (photons/s)	$9.2 \times 10^3$	$4.1 \times 10^2$	$5.2 \times 10^3$	$1.9 \times 10^3$	$8.8 \times 10^3$	$3.1 \times 10^2$

<sup>A</sup> Integrated reflectivity scaled to Ge(220) via values of  $R_{\text{obs}}$  in Table 1.

## 6. Intensity Calculations

To illustrate the compromise between resolution (equations 1–3) and intensity (equations 9–14), calculations of absolute integrated intensities (defined as  $\Sigma i$ , the total counts under the peak minus background) and the peak counting rate (defined in equation 14) have been made for six scattering configurations and the (220) reflection from two reference samples, Si and CeO<sub>2</sub>, which have relatively low and high absorption coefficients (141 and 2076 cm<sup>-1</sup> respectively at  $\lambda = 1.54 \text{ \AA}$ ). The

calculations have been made for flat-plate (FP) and capillary samples as indicated in Table 3. An incident beam of wavelength  $1.54 \text{ \AA}$  containing  $2 \times 10^{10}$  photons/s in an area  $4 \times 1 \text{ mm}$  was assumed. This is a conservative number, since as previously mentioned an order of magnitude higher intensity should not be difficult to achieve.

Table 3 demonstrates that the total counts for the flat-plate sample of Si range from  $5 \times 10^4 \text{ s}^{-1}$  if a Ge(220) analyser is used to  $1.9 \times 10^5 \text{ s}^{-1}$  for an  $0.2 \text{ mm}$  receiving slit. About one-half these counting rates are obtained for the heavily absorbing flat-plate sample of  $\text{CeO}_2$ . However, the much narrower peak widths obtained with the analyser crystals are reflected in proportionally higher peak counting rates,  $1.6 \times 10^4 \text{ s}^{-1}$  for LiF(400) against  $1.7 \times 10^4 \text{ s}^{-1}$  for the receiving slit. Counting statistics at this level are more than sufficient for most Rietveld analyses.

The calculations for the capillary samples are based upon a diameter of  $0.2 \text{ mm}$  and a packing density of 30%, except for Si used with the two analysers, where the low absorption makes it possible to take advantage of the fact that a  $1 \text{ mm}$  diameter sample can be used with no loss of resolution. The counting rates for the latter are about 40% of those obtained with flat-plate geometry. The capillary technique under these conditions therefore provides a very useful option, for example to eliminate preferred orientation (Thompson *et al.* 1987) or if the sample is air or moisture-sensitive, provided it is not too strongly absorbing. This is evident from the respective counting rates for the  $0.2 \text{ mm}$   $\text{CeO}_2$  capillaries, which are a factor of 25 lower than the corresponding flat-plate figures.

The counting rates for the PSD with a  $0.2 \text{ mm}$  capillary are especially interesting. Although these appear to be significantly lower, a direct comparison does not take into account the simultaneous data collection over a relatively wide angular range. For example, in the experiments reported by Lehmann *et al.* (1987) a range of  $2.7^\circ$  was covered for each 'step' of the PSD, corresponding to 270 points on a normal step-scan at  $0.01^\circ$  intervals with a conventional detector, giving an enhancement factor of one to two orders of magnitude.

The experimentally observed intensities for Si(220) flat-plate samples with Ge(220) and LiF(400) analysers are routinely found to be about 60% of the calculated values in Table 3. This difference can be largely accounted for by attenuation losses through air, mylar windows, the Be window of the detector, and the omission of an absorption correction in the reflectivity calculated from equation (12). These factors should be taken into account in more precise calculations (Suortti *et al.* 1985).

## 7. Concluding Remarks

Although synchrotron X-ray powder diffraction is still in its early stages of development, the acquisition of high quality reproducible data presents no difficulty. For a given scattering configuration the instrumental resolution function can be determined from very simple considerations, and absolute intensities can be calculated with reasonable accuracy. This permits optimisation of the scattering geometry for any particular experiment. If high resolution and low background are required, the crystal-analyser technique offers several advantages, but for experiments where high intensity is at a premium, and more relaxed collimation can be tolerated, Soller receiving slits may be more advantageous. For rapid collection of high resolution data where background is not an important consideration, a linear PSD is a very attractive alternative if available.

Careful attention needs to be given to appropriate characterisation of the sample before synchrotron data are collected. The resolution of the pattern may be significantly degraded if the particle size is much less than 1  $\mu\text{m}$  or if there is substantial microscopic strain. The possibility of using wide-diameter capillaries is a very useful option to keep in mind for some experiments. For materials such as  $\text{CeO}_2$  which are highly absorbing at 1.54  $\text{\AA}$ , there is always the possibility of working at shorter wavelengths; for example, at 0.7  $\text{\AA}$  the value of  $\mu$  for  $\text{CeO}_2$  is only  $273\text{ cm}^{-1}$ .

In most cases, peak shapes appear to be adequately described by the convolution of Gaussian and Lorentzian functions, and the angular variation of the peak widths can be represented by simple expressions. There is thus in general no obstacle to the use of standard techniques of profile analysis, either Rietveld structure refinement or decomposition into integrated intensities for subsequent application of *ab initio* methods of analysis; both approaches have been used successfully in several cases. However, there are exceptions for which the peak shapes do not conform to this simple model, and more detailed analysis of line broadening is needed in these cases. There is also an urgent need for the development of generalised models of anisotropic line broadening and preferred orientation which can be readily incorporated into existing software for profile analysis.

Rapid progress can be expected in the next two years as additional powder facilities come on-line at other synchrotron sources (see elsewhere in this issue). Substantial gains in intensity can be realised with improved focussing optics, and minimisation of line-broadening due to wavelength dispersion with appropriately curved monochromators should lead to significantly improved resolution. The use of multiple detector systems similar to those which are standard on high resolution neutron diffractometers is a simple method of improving the efficiency of data collection. Curved PSDs covering very wide angular ranges are another very promising, albeit expensive, approach. In this context, film cameras should not be overlooked as a very inexpensive and simple alternative.

### Acknowledgments

We would like to thank P. Suortti for a critical reading of the manuscript and several helpful suggestions. We are also grateful to R. Sabatini for obtaining SEM pictures of the Si standard. One of us (D.E.C.) acknowledges the support of the Division of Materials Sciences, US Department of Energy, under contract DE-AC02-76CH00016.

### References

- Attfield, J. P., Cheetham, A. K., Sleight, A. W., and Cox, D. E. (1986*a*). NSLS Annual Report, pp. 315–16, Brookhaven National Laboratory.
- Attfield, J. P., Sleight, A. W., and Cheetham, A. K. (1986*b*). *Nature* **322**, 620–2.
- Caglioti, G., Paoletti, A., and Ricci, F. P. (1958). *Nucl. Instrum. Methods* **3**, 223–8.
- Caglioti, G., and Tocchetti, D. (1965). *Nucl. Instrum. Methods* **32**, 181–9.
- Christensen, A. N., Lehmann, M. S., and Nielsen, M. (1985). *Aust. J. Phys.* **38**, 497–505.
- Cox, D. E., Hastings, J. B., Cardoso, L. P., and Finger, L. W. (1986). In 'Materials Science Forum', Vol. 9 (Ed. C. R. A. Catlow), pp. 1–20 (Trans. Techn. Publications: Switzerland).
- Cox, D. E., Hastings, J. B., Thomlinson, W., and Prewitt, C. T. (1983). *Nucl. Instrum. Methods* **208**, 573–8.
- Hastings, J. B., Thomlinson, W., and Cox, D. E. (1984). *Acta Crystallogr.* **17**, 85–95.
- Hewat, A. W. (1973). U.K. A.E.R.E. Report RRL73/897, Harwell.
- Hewat, A. W. (1975). *Nucl. Instrum. Methods* **127**, 361–70.

- Hewat, A. W. (1979). *Acta Crystallogr. A* **35**, 248.
- Jennings, L. D. (1984). *Acta Crystallogr. A* **40**, 12–16.
- Kasper, J. S., and Lonsdale, K. (Eds) (1959). 'International Tables for X-ray Crystallography', Vol. II, pp. 291–9 (Kynoch Press: Birmingham).
- Lehmann, M. S., Christensen, A. N., Fjellvag, H., Feidenhans'l, R., and Neilsen, M. (1987). *J. Appl. Crystallogr.* **20**, 123–9.
- McKeown, D. A., Prewitt, C. T., and Cox, D. E. (1986). NLS Annual Report, pp. 329–30, Brookhaven National Laboratory.
- Marezio, M., Rossel, C., and Cox, D. E. (1988). (to be published).
- Materlik, G., and Suortti, P. (1984). *J. Appl. Crystallogr.* **17**, 7–12.
- Parrish, W., and Hart, M. (1985). *Trans. Am. Crystallogr. Assoc.* **21**, 51–5.
- Parrish, W., Hart, M., Erickson, C. J., Masciocchi, N., and Huang, T. C. (1986*a*). *Adv. X-ray Anal.* **29**, 243–50.
- Parrish, W., Hart, M., and Huang, T. C. (1986*b*). *J. Appl. Crystallogr.* **19**, 92–100.
- Rietveld, H. M. (1969). *J. Appl. Crystallogr.* **2**, 65–71.
- Rouse, K. D., Cooper, M. J., York, E. J., and Chakera, A. (1970). *Acta Crystallogr. A* **26**, 682–91.
- Smith, G. S., Johnson, Q. C., Cox, D. E., Snyder, R. L., Smith, D. K., and Zalkin, A. (1987). *Adv. X-ray Anal.* **30**, 383–8.
- Suortti, P., Hastings, J. B., and Cox, D. E. (1985). *Acta Crystallogr. A* **41**, 413–16.
- Thompson, P., Cox, D. E., and Hastings, J. B. (1987). *J. Appl. Crystallogr.* **20**, 79–83.
- Wertheim, G. K., Butler, M. A., West, K. W., and Buchanan, D. N. E. (1974). *Rev. Sci. Instrum.* **45**, 1369–71.
- Young, R. A., and Wiles, D. B. (1982). *J. Appl. Crystallogr.* **15**, 430–8.

Manuscript received 21 August, accepted 2 November 1987

